Full Dimensional (15D) Quantum-Dynamical Simulation of the Protonated Water-Dimer II: Infrared Spectrum and Vibrational Dynamics.

Oriol Vendrell, Fabien Gatti, H.-D. Meyer

Full Dimensional (15D) Quantum-Dynamical Simulation of the Protonated Water-Dimer II: Infrared Spectrum and Vibrational Dynamics

Oriol Vendrell,[1,*] Fabien Gatti,[2,†] and Hans-Dieter Meyer[1,‡]

[1] *Theoretische Chemie, Physikalisch-Chemisches Institut, Universität Heidelberg, INF 229, D-69120 Heidelberg, Germany*

[2] *LDSMS (UMR 536-CNRS), CC 014, Université de Montpellier II, F-34095 Montpellier, Cedex 05, France*

(Dated: November 15, 2018)

Abstract

The infrared absorption spectrum of the protonated water dimer ($H_5O_2^+$) is simulated in full dimensionality (15D) in the spectral range 0–4000 cm^{-1}. The calculations are performed using the Multiconfiguration Time-Dependent Hartree (MCTDH) method for propagation of wavepackets. All the fundamentals and several overtones of the vibrational motion are computed. The spectrum of $H_5O_2^+$ is shaped to a large extent by couplings of the proton-transfer motion to large amplitude fluxional motions of the water molecules, water bending and water-water stretch motions. These couplings are identified and discussed, and the corresponding spectral lines assigned.

The large couplings featured by $H_5O_2^+$ do not hinder, however, to describe the coupled vibrational motion by well defined simple types of vibration (stretching, bending, etc.) based on well defined modes of vibration, in terms of which the spectral lines are assigned. Comparison of our results to recent experiments and calculations on the system is given. The reported MCTDH IR-spectrum is in very good agreement to the recently measured spectrum by Hammer *et al.* [JCP, **122**, 244301, (2005)].

*e-mail: oriol.vendrell@pci.uni-heidelberg.de

†e-mail: gatti@univ-montp2.fr

‡e-mail: Hans-Dieter.Meyer@pci.uni-heidelberg.de

I. INTRODUCTION

The understanding of the hydrated proton in bulk water and water-containing systems is of importance to many areas in chemistry and biology. Much effort has been directed in recent years towards obtaining a better understanding of the excess proton in water and important contributions have appeared due to the advance in experimental and theoretical techniques [1, 2, 3, 4, 5].

The importance of the hydrated proton and the amount of work devoted to the problem contrast with the fact that the smallest system in which a proton is shared between water molecules, the protonated water dimer ($H_5O_2^+$), is not yet completely understood, and an explanation of some important spectral signatures and an overall picture of the dynamics of the cation is lacking. Accurate infrared (IR) spectroscopy of protonated water clusters prepared in the gas phase has become possible in recent years [4, 5, 6, 7, 8], opening the door to a deeper understanding of these systems and the hydrated proton in general.

The protonated water dimer, $H_5O_2^+$, also known as Zundel cation, is the smallest protonated water cluster, and has been recently object of intense study. The infrared (IR) spectrum of the system has been measured in the gas phase, either using multiphoton dissociation techniques [6, 7] or measuring the vibrational predissociation spectrum of $H_5O_2^+ \cdot RG_n$ clusters with RG=Ar,Ne [5, 8]. The obtained spectra could not be consistently assigned in terms of fundamental frequencies and overtones of harmonic vibrational modes due to large-amplitude anharmonic displacements and couplings of the cluster. Hence, more sophisticated theoretical approaches are required. Several theoretical studies have been conducted over the last years in order to understand and assign the IR spectrum of the cation [5, 9, 10, 11, 12, 13, 14, 15].

The first measurement [6] of the IR multiphoton dissociation spectrum (IRMPD) of $H_5O_2^+$ spanned the range between 620 and 1900 cm^{-1}. Three main absorptions were discussed and assigned, based on a previous quantum-dynamical simulation of the IR absorption spectrum on a 4D model of the hydrogen-bond (O-H-O) fragment [9]. Those assignments were revisited in the context of newer IRMPD experiments and calculations, producing somewhat disparate results [5, 7, 12, 13]. Recent measurements of the IR predissociation spectrum of the $H_5O_2^+$ cation in argon-solvate [8] and neon- and argon-solvate [5] conditions present spectra with a simpler structure than the multiphoton IRMPD ones. It is expected

that the spectrum of the $H_5O_2^+ \cdot Ne_1$ complex is close to the linear absorption spectrum of the bare cation [5]. This spectrum features a doublet structure in the region of 1000 cm^{-1} made of two well-defined absorptions at 928 cm^{-1} and 1047 cm^{-1}. This doublet structure was not fully understood until recently, although the highest-energy component had been already assigned by Bowman and collaborators to the asymmetric proton-stretch fundamental ([O-H-$O_{\|}$]) [5]. A similar argument was made by Sauer and collaborators based on classical-trajectories calculations [12]. In this respect, it is known from recent classical-dynamics simulations on accurate potential energy surfaces (PES) that the [O-H-$O_{\|}$] motion features large amplitude displacements strongly coupled to other modes of the system. The central-proton displacement would then be involved in most of the lines appearing in the IR spectrum, since this motion contributes the largest changes in the dipole moment of the cation [12, 13]. Recent work by us assigns unambiguously the doublet for the first time [14], which is shown to arise from the coupling of low-frequency motions of the water molecules to the central proton motion.

In this work we undertake the simulation of the IR spectrum and dynamics of $H_5O_2^+$ using the multiconfiguration time-dependent Hartree (MCTDH) [16, 17, 18] method. In doing so we do not rely on a low-dimensional model of the system, but we treat it in its full (15D) dimensionality. The obtained IR spectrum is compared to recent experimental and theoretical results [5]. The experimental IR spectrum and our results agree well in the position and relative intensities of the main spectral features, which allows us to extract meaningful conclusions regarding the dynamics of the cluster. All fundamentals and several overtones of the vibrational motion of the cation are computed and their properties analyzed. The computation of vibrational states in terms of their fully correlated wavefunctions is invaluable in the assignment of spectral lines arising from the time-dependent computation of the IR spectrum.

The reported simulations are performed using curvilinear coordinates, which has been found crucial for the description of the large amplitude motions and anharmonicities featured by the cluster [15]. A description of the derivation of the exact kinetic energy operator (KEO) in this set of coordinates and of the representation of the potential energy surface (PES) are discussed in the companion paper [15], hereafter referred to as Paper I. The quality of the PES expansion, and the properties of the ground-vibrational state of the system are also analyzed in Paper I. The reference PES and dipole moment surfaces (DMS) used are those

of Huang et al. [11], which constitute the most accurate *ab initio* surfaces available to date for this system.

II. THEORY AND METHODS

The quantum-dynamical problem is solved using the multiconfiguration time-dependent Hartree (MCTDH) method [16, 17, 18]. For a brief description of MCTDH see Paper I. All the reported simulations were performed with the Heidelberg MCTDH package of programs [19].

The definition of the system of curvilinear coordinates used in the description of $H_5O_2^+$ is given in Paper I. The 15 internal coordinates are briefly reintroduced here to make the discussion self-contained. These are: the distance between the centers of mass of both water molecules (R), the position of the central proton with respect to the center of mass of the water dimer (x,y,z), the Euler angles defining the relative orientation between the two water molecules (waggings: γ_A, γ_B; rockings: β_A, β_B; internal relative rotation: α) and the Jacobi coordinates which account for the particular configuration of each water molecule ($R_{1(A,B)}, R_{2(A,B)}, \theta_{(A,B)}$)) where R_{1x} is the distance between the oxygen atom and the center of mass of the corresponding H_2 fragment, R_{2x} is the H–H distance and θ_x is the angle between these two vectors. The grouping of the coordinates into modes is discussed in Paper I. Here we repeat only the mode-combination scheme used. The coordinates have been grouped into the following five combined modes: $Q_1 = [z, \alpha, x, y]$, $Q_2 = [\gamma_A, \gamma_B]$, $Q_3 = [R, u_{\beta_A}, u_{\beta_B}]$, $Q_4 = [R_{1A}, R_{2A}, u_{\theta_{1A}}]$ and $Q_5 = [R_{1B}, R_{2B}, u_{\theta_{1B}}]$.

A. IR Spectrum calculation in the MCTDH framework

The IR absorption cross-section is given by [20]:

$$I(E) = \frac{\pi E}{3\, c\, \epsilon_0\, \hbar} \sum_n |\langle \Psi_n | \Psi_{\mu,0} \rangle|^2 \, \delta(E + E_0 - E_n), \tag{1}$$

where $|\Psi_{\mu,0}\rangle$ is the dipole-operated initial state, i.e., $|\Psi_{\mu,0}\rangle \equiv \hat{\mu}\,|\Psi_0\rangle$, and E_0 is the ground-state energy. The IR spectrum may be equivalently computed in the time-dependent picture.

From Eq. (1) follows

$$I(E) = \frac{E}{6\,c\,\epsilon_0\,\hbar^2}\int_{-\infty}^{\infty} e^{i(E+E_0-E_n)t/\hbar}\langle\Psi_{\mu,0}|\Psi_n\rangle\ \langle\Psi_n|\Psi_{\mu,0}\rangle\ dt \tag{2a}$$

$$= \frac{E}{6\,c\,\epsilon_0\,\hbar^2}\int_{-\infty}^{\infty} e^{i(E+E_0)t/\hbar}\langle\Psi_{\mu,0}|e^{-i\,H\,t/\hbar}|\Psi_{\mu,0}\rangle\ dt \tag{2b}$$

$$= \frac{E}{3\,c\,\epsilon_0\,\hbar^2}\,Re\int_{0}^{\infty} e^{i(E+E_0)t/\hbar}a_\mu(t)\ dt, \tag{2c}$$

where the autocorrelation function of the dipole-operated initial state, $a_\mu(t)$, has been defined in Eq. (2c) implicitly. The real part, Re, appears because $a_\mu(-t) = a_\mu^*(t)$ holds. Eq. (2c) tells that the IR spectrum is obtained in the time-dependent picture by Fourier transformation (FT) of the autocorrelation of the dipole-operated initial state. Whether a time-dependent or a time-independent approach is more efficient depends on the problem at hand. A time-independent approach relies on the accurate computation of the eigenstates of the Hamiltonian, $|\Psi_n\rangle$, which may be accomplished by iterative-diagonalization methods of the Hamiltonian matrix expressed in some basis, obtaining all the eigenstates up to some desired energy, and then using Eq. (1) to compute the IR spectrum. The method to obtain eigenstates of the Hamiltonian within the MCTDH approach is called *improved relaxation* [21] and consists essentially on a time-independent multiconfiguration self consistent field (MCSCF) computation of an eigenstate, in which both the expansion coefficients of the wavefunction and the basis of SPFs (see Eq. (1) in Paper I) are optimized to self-consistency. The optimal basis of SPFs varies from state to state, which difficults the application of iterative diagonalization procedures to the computation of the whole spectrum. To obtain each excited state with *improved relaxation*, a new computation is needed in which the basis is optimized for that specific state. A comprehensive calculation of an IR spectrum by *improved relaxation* has been recently achieved for 6D problems, namely H_2CS [21], and HONO [22]. The lowest 184 states of A' symmetry of the latter molecule were calculated. The *improved relaxation* approach, however, is not practicable with the current computational capabilities to obtain the whole spectrum for a molecule of the size of $H_5O_2^+$. The iterative process of improved relaxation converges only if the space spanned by the configurations allows to separate the desired state from neighboring ones. When the density of states increases, the number of SPFs necessary to ensure convergence increases as well. This makes it impossible to compute states higher in energy. For the present problem we could compute states up to about 600 cm^{-1}. However, not only the excitation energy

but also state coupling determines the feasibility of improved relaxation. For example, we could compute the second excited state of the water-water stretch by *improved relaxation*, despite its excitation energy is 1069 cm^{-1}.

Propagation of a wavepacket by MCTDH, on the other hand, is always feasible. A small set of SPFs makes a propagation less accurate, but not impossible. Therefore, the full IR spectrum is efficiently calculated in the time-dependent representation. The resolution at which different peaks of the spectrum are resolved is given by the Fourier Transform (FT) of the damping function $g(t)$ [17] with which the autocorrelation $a_\mu(t)$ is to be multiplied when performing the integral (2c) to minimize artifacts due to the Gibbs phenomenon. We choose $g(t) = \cos(\pi t/2T)$ and set $g(t) = 0$ for $t > T$, where T denotes the length of the autocorrelation function. Since we make use of the $T/2$ trick, $a_\mu(t) = \langle \Psi^*_{\mu 0}(t/2) | \Psi_{\mu 0}(t/2) \rangle$, which holds when the initial wavepacket is real and the Hamiltonian symmetric, T is twice the propagation time. The FT of $g(t)$ is known [17] and its full width at half maximum (FWHM) is

$$\Delta E = 27,300 \text{ cm}^{-1} \text{ fs } /T. \tag{3}$$

To clearly identify two peaks 100 cm^{-1} apart, i.e., the doublet structure in the $H_5O_2^+$ spectrum, one needs a resolution of $\Delta E = 67$ cm^{-1} and hence a propagation time of $T/2 = 200$ fs. Time propagations have been carried out over 500 fs providing a resolution of 30 cm^{-1}.

Often we make use of the filter diagonalization (FD) technique [23, 24, 25, 26] to analyze the autocorrelation function of the propagated wavepackets, which yields eigenenergies and spectral intensities. FD is able to provide accurate eigenenergies from shorter time propagations than the ones needed to resolve the IR spectrum. However, FD calculations are more sensitive to errors in the autocorrelation function compared to the FT method. Therefore these calculations are targeted to obtain accurate energies of a single state or a small group of related states from a propagation of an appropriately prepared initial wavepacket.

The dipole operator is a vector and the operator $\hat{\mu}$ appearing in Eqs. (1,2) is to be interpreted as the scalar product $\vec{e} \cdot \vec{\hat{\mu}}$ where $\vec{e}$ denotes the polarization vector of the absorbed light. As the molecule is assumed to be randomly oriented we average over all orientations and obtain

$$I(E) = \frac{1}{3}(I_z(E) + 2I_x(E)), \tag{4}$$

where I_z and I_x denote the intensities obtained with the $x-$ and $z-$component of the dipole

operator, respectively. The factor 2 appears because $a_{\mu_x} = a_{\mu_y}$ holds. The intensity I_y is hence not explicitly computed.

B. Eigenstates of the system and spectrum assignment

Even if the computation of the IR spectrum in the time-dependent representation is feasible, a means of assigning the different lines to specific motions of the system is still required.

Wavefunctions of excited states converged by *improved relaxation* [21] contain all the possible information of that specific state. The intensity of a given excited state $|\Psi_n\rangle$ is readily obtained by computing the dipole moment $|\langle\Psi_n|\hat{\mu}|\Psi_0\rangle|^2$. But even if an excited state of interest $|\Psi_n\rangle$ has been obtained it is difficult to directly inspect these mathematical objects due to their high dimensionality. Moreover, for the higher excited states we do not have $|\Psi_n\rangle$ at our disposal but only an autocorrelation function providing spectral lines. In both cases we characterize the eigenstates by their overlaps with carefully chosen test states, i.e., by the numbers $|\langle\Phi_{test}|\Psi_n\rangle|^2$. The following procedures are used:

1. Test states $|\Phi_{test}\rangle$ are generated

   a) by applying some operator $\hat{O}$ to a previously converged eigenfunction,

   $$|\Phi_{test}\rangle = N\hat{O}|\Psi_n\rangle, \tag{5}$$

   where N is a normalization constant, e.g., $N\hat{z}|\Psi_0\rangle$ generates a test state which in essence differs from the ground state $|\Psi_0\rangle$ by a one quantum excitation in the proton-transfer coordinate z.

   b) by forming Hartree products, where the SPFs are obtained through diagonalization of mode-Hamiltonians $\hat{h}_j$. The $\hat{h}_j$ are low-dimensional Hamiltonians and each $\hat{h}_j$ operates on the space of a group of coordinates (see Paper I for details on coordinates grouping into modes). Rather than using single Hartree products one may use linear combinations of products in order to satisfy a symmetry constraint.

2. The overlaps $|\langle\Phi_{test}|\Psi_n\rangle|^2$ are then computed by

a) by direct evaluation of the scalar product if $|\Psi_n\rangle$ is available.

b) by Fourier transform of the autocorrelation function $a(t) = \langle\Phi_{test}|\exp(-i\ H\ t)|\Phi_{test}\rangle$. The overlap is obtained via the formula [21]:

$$|\langle\Phi_{test}|\Psi_n\rangle|^2 = \frac{\pi}{2T} Re \int_0^T e^{iE_n t} a(t) \cos(\frac{\pi t}{2T}) dt \tag{6}$$

c) by Fourier transformation of the cross-correlation function $c(t) = \langle\Phi_{test}|\exp(-i\ H\ t)|\Psi_{\mu,0}\rangle$. The absolute square of the FT of $c(t)$ at energy E_n must then be divided by the spectral intensities of $|\Psi_{\mu,0}\rangle$ to obtain $|\langle\Phi_{test}|\Psi_n\rangle|^2$. This is the fastest method because it does not require additional propagations. However, it is also the least accurate procedure. We used this method several times to obtain a quick overview, but it was not used to generate data reported in this article.

Excitations related to test states will be denoted $(n_1\, q_1, n_2\, q_2 \ldots)$, where n_1 represents the quanta of excitation on coordinate q_1 (in a separable limit). A test state will be denoted by $|\Phi_{n_1\, q_1, n_2\, q_2 \ldots}\rangle$ where the terms with $n_j = 0$ are omitted. In case a test state has been generated such that it cannot be represented by this simple notation, it will be defined more explicitly.

III. RESULTS AND DISCUSSION

FIGURE 1 AROUND HERE

FIGURE 2 AROUND HERE

The MCTDH spectrum in the full range 0–4000 cm^{-1} is depicted in Fig. 1 and compared to experiment in Fig. 2. The dipole-moment operated ground state $\hat{\mu}|\Psi_0\rangle$ was propagated for 500 fs, yielding an autocorrelation of 1000 fs. The spectrum was calculated according to Eq. (2) and the FWHM resolution of the spectrum is, according to Eq. (3), about 30 cm^{-1}.

In the following sections the different parts of the spectrum and the peak assignments are discussed. Table I collects the energies of several states of $H_5O_2^+$ obtained with MCTDH, MULTIMODE [5] and experimental values on the $H_5O_2^+$·Ne system [5].

TABLE I AROUND HERE

The symmetry labels of the discussed vibrational states are given within the $\mathcal{G}_{16}$ symmetry group, which arises due to the feasibility (in the sense of Longet-Higgins [27]) of the wagging and internal rotation motions (see Paper I). A character table for the $\mathcal{G}_{16}$ symmetry group is found in Table A-25 in Ref. [28]. If the internal rotation motion around α is assumed to be unfeasible, the symmetry analysis can be performed using the $\mathcal{D}_{2d}$ point group. The permutation-inversion group $\mathcal{G}_{16}$ contains the $\mathcal{D}_{2d}$ point group as a subgroup, but allows additionally to permute the two hydrogens of one of the water monomers [28, 29]. The $\mathcal{G}_{16}$ labels reduce to the $\mathcal{D}_{2d}$ ones by ignoring $(-/+)$ signs in the labeling provided by $\mathcal{G}_{16}$. The use of $\mathcal{G}_{16}$ becomes important when labeling the states related to the internal rotational motion. The z component of the dipole moment excites vibrational states of B_2^+ symmetry, while the perpendicular components those of E^+ symmetry.

A. Low-energy region

The low energy region of the spectrum, below 900 cm^{-1}, has not yet been accessed experimentally. The reported spectrum in Fig. 1 shows a strong absorption around 100 cm^{-1} followed by two lines of fewer intensity at about 250 and 500 cm^{-1}, respectively. The three absorptions arise from excitation of the perpendicular component of the field. Modes oscillating at these low frequencies are strongly anharmonic: already in the ground vibrational state, the system interconverts between equivalent minima through low barriers along the wagging (γ_A, γ_B) and torsional (α) coordinates [15].

FIGURE 3 AROUND HERE

The first three excited states associated to the internal rotation (1α, 2α, 3α) have been computed with *improved relaxation* and their probability-density along the internal rotation α is depicted in Fig. 3. The energy of the (4α) state has been computed by FD. They have excitation energies of 1, 103, 126 and 210 cm^{-1}, and symmetries A_1^-, B_1^+, B_1^- and A_1^+, respectively. Here (1α) is the splitting state related to the torsional barrier along α. The excitation energy of 1 cm^{-1} is hence the tunneling split. In fact, the symmetry label of the rotationally-split state of a (+) state is obtained by multiplication with A_1^-.

FIGURE 4 AROUND HERE

FIGURE 5 AROUND HERE

Fig. 4 depicts the probability-density projection on the wagging coordinates for the ground vibrational state, which is of A_1^+ symmetry, as well as for one of the two fundamental states (w_{1a},w_{1b}) of the wagging modes. The fundamental wagging modes are centered at 106 cm^{-1} and belong to the E^- irreducible representation of the $\mathcal{G}_{16}$ group. Therefore, they are doubly degenerate, dark states. The band at about 100 cm^{-1} (see Fig. 1 center) due to the perpendicular component of the dipole corresponds to the states centered at 108 cm^{-1}, which belong to the E^+ irreducible representation. Such states are combined states of the fundamental wagging motion and the (1α) state of the internal rotation, of A_1^- symmetry. Thus, both pairs of degenerate wagging states, centered at 106 and 108 cm^{-1} are split states with respect to the internal rotational barrier around α. In a similar way the band at about 250 cm^{-1} corresponds to the combination of the fundamental wagging motion and the (3α) internal-rotation state, which belongs to the B_1^- irreducible representation. This combination results in two degenerate states of E^+ symmetry. The energies of the next three wagging-mode states (w_2,w_3,w_4) are, respectively, 232, 374 and 422 cm^{-1} and they are shown in Figs. 5a, 5b and 5c, respectively. These three states correspond to two quanta of excitation in the wagging motions and they can be represented by kets $|11\rangle$, $(|20\rangle - |02\rangle)/\sqrt{2}$ and $(|20\rangle + |02\rangle)/\sqrt{2}$, respectively, where the $|ab\rangle$ notation signifies the quanta of excitation in the wagging motions of monomer A and B. These states have symmetries B_1^+, B_2^+ and A_1^+, respectively. In the harmonic limit these three states would be degenerate. The next 2 states, w_{4a},w_{4b}, which are not computed, are degenerate again and correspond to kets $|31\rangle$ and $|13\rangle$. State w_2 has an energy that nearly doubles the energy of the w_{1x} states, since it roughly corresponds to one quantum in state w_{1a} and one quantum in state w_{1b}. The strong anharmonicity of the wagging motions as well as the coupling between right and left wagging can be further appreciated in the progression of w_2, w_3 and w_4 vibrational-state energies. We emphasize again that these three states are degenerate in the harmonic limit. In addition, the harmonic-analysis energies of the two lowest wagging-fundamentals w_{1a} and w_{1b} are around 300 cm^{-1} larger than the MCTDH result and do not account for their degeneracy, since harmonic normal-modes are constructed taking as a reference the $\mathcal{C}_2$ absolute minimum. However, as discussed above and in Paper I, $H_5O_2^+$ interconverts through low potential barriers between several equivalent minima and has $\mathcal{G}_{16}$

symmetry. The state w_3 has four probability-density maxima along the 2D space spanned by γ_A and γ_B. They correspond to geometries in which one of the water molecules adopts a trigonal-planar geometry (H_3O^+ character) and the other adopts a pyramidal geometry (H_2O character). This state transforms according to the B_2^+ symmetry representation, which is also the symmetry of the proton-transfer fundamental. State w_3 will play a major role due to its strong coupling to the proton-transfer mode.

The first two fundamentals of the symmetric stretch ([O-$O_{\|}$], R coordinate) have energies of 550 and 1069 cm^{-1} respectively, and have A_1^+ symmetry, while the rocking fundamentals, which are degenerate E^+ states, have an energy of 481 cm^{-1} and are responsible of the band appearing slightly below 500 cm^{-1} in the MCTDH spectrum. In contrast to the wagging motion, the rocking motion is fairly harmonic and exhibits only a weak coupling between left and right rocking. The energies of the two-quanta rocking states r_2, r_3 and r_4 – defined in a similar way to w_2, w_3 and w_4 but with a reverse ordering of the zero-order *ket*-states – are therefore almost degenerate. These energies read 915, 930 and 943 cm^{-1}.

B. Doublet at 1000 cm^{-1}

The doublet centered at 1000 cm^{-1} is the most characteristic feature of the IR spectrum of $H_5O_2^+$. It is depicted in Fig. 2 (top). The highest energy line has been measured to be at 1047 cm^{-1} while the low energy component appears at 928 cm^{-1} [5]. There is accumulated evidence in the literature that the absorption of the proton-transfer fundamental occurs in the region of 1000 cm^{-1} [5, 10, 11, 12, 13]. Specifically, the band at 1047 cm^{-1} in Ref. [5] was assigned to the first excitation of the central proton motion [5] based on MULTIMODE [30] calculations. This band is the most intense band of the spectrum since the central proton motion along the z axis induces a large change in the dipole-moment of the cation. The low-energy component has been recently assigned by us [14]. The doublet is seen to arise from coupling between the proton-transfer motion [O-H-$O_{\|}$], the low frequency water-wagging modes and the water-water stretching [O-$O_{\|}$] motion. In order to obtain a fundamental understanding of the low-energy ($|\Psi_d^l\rangle$) and high energy ($|\Psi_d^h\rangle$) components of the doublet, test states were constructed by operating with $\hat{z}$ on the ground state: $|\Phi_{1z}\rangle = \hat{z}|\Psi_0\rangle N$, where N is a normalization constant, and by operating with $(\hat{R} - R_0)$ on the third excited wagging state w_3: $|\Phi_{1R,w_3}\rangle = (\hat{R} - R_0)|\Psi_{w_3}\rangle N$. Note that $|\Phi_{1z}\rangle$ is characterized by one

quantum of excitation in the proton-transfer coordinate whereas $|\Phi_{R1,w_3}\rangle$ by one quantum in [O-O$_{\|}$] and two quanta in the wagging motion. These two test states were propagated and their auto- and crosscorrelation functions were used for FD analysis, which yielded an energy of 918 cm^{-1} for $|\Psi_d^l\rangle$ and an energy of 1033 cm^{-1} for $|\Psi_d^h\rangle$. These energies are in good accordance to the peaks in Fig. 2 which arise from the propagation of $|\Psi_{\mu,0}\rangle$. The spectral intensities were also obtained by FD analysis. The overlaps of the test states to the states making the doublet read: $|\langle\Phi_{1z}|\Psi_d^l\rangle|^2 = 0.09$, $|\langle\Phi_{1R,w_3}|\Psi_d^l\rangle|^2 = 0.83$ and $|\langle\Phi_{1z}|\Psi_d^h\rangle|^2 = 0.46$, $|\langle\Phi_{1R,w_3}|\Psi_d^h\rangle|^2 = 0.10$. One should take into account that these numbers depend on the exact definition of the test states, which is not unique. However, they provide a clear picture of the nature of the doublet: the low-energy band has the largest contribution from the combination of the symmetric stretch and the third excited wagging (see Figs. 5b and 3c), whereas the second largest is the proton-transfer motion. For the high-energy band the importance of these two contributions is reversed. Thus, the doublet may be regarded as a Fermi-resonance between two zero-order states which are characterized by ($1R$, w_3) and ($1z$) excitations, respectively. The reason why the third wagging excitation plays an important role in the proton-transfer doublet is understood by inspecting Fig. 5b and 6. The probability density of state w_3 has four maxima, each of which corresponds to a planar conformation of H_2O-H^+ (H_3O^+ character) for one of the waters, and a bent conformation (H_2O character) where a lone-pair H_2O orbital forms a hydrogen bond with the central proton. When the proton oscillates between the two waters, the two conformations exchange their characters accordingly. Thus, the asymmetric wagging mode (w_3, 374 cm^{-1}) combines with the water-water stretch motion (R, 550 cm^{-1}) to reach an energy close to the natural absorption-frequency of the proton transfer, making these motions coupled. The two states of the doublet transform according to the B_2^+ irreducible representation of $\mathcal{G}_{16}$.

One last remark regarding the spectral region of the doublet is the small but noticeable absorption, which is appreciated both in the experimental and MCTDH spectra between both peaks (see Fig. 2). This low-intensity absorption is due to the r_3 rocking centered at 930 cm^{-1} and which belongs to the B_2^+ irreducible representation. In an analogous way to the w_3 wagging state, the r_3 rocking state presents four probability-density maxima along the rocking coordinates, each of which consists of one water aligned with the central axis while the other is in a bent conformation, and therefore will present some degree of coupling to the proton-transfer motion. The low absorption of this band, despite its proximity to

the natural absorption-frequency of the proton-transfer motion, is qualitatively explained by the fact that the rocking motions do not change the hybridization properties of the water monomers and are of a lower amplitude in comparison to the wagging motions. The rocking motion hence couples more weakly to the proton-transfer motion and induces a smaller change of the dipole-moment as compared to the wagging motions.

FIGURE 6 AROUND HERE

C. 1000-2000 cm^{-1} region

The region between the proton-transfer doublet and the doublet centered at 1800 cm^{-1} features couplings related to the [O-H-O$_{\|}$] and [O-O$_{\|}$] motions. The MCTDH spectrum reported in Fig. 1 presents three main absorptions in this range, located at 1411, 1741 and 1898 cm^{-1}. We call the eigenstates producing these peaks $|\Psi_{m1}\rangle$, $|\Psi_{m2}\rangle$ and $|\Psi_{m3}\rangle$, respectively, where the m stands for middle spectral-range. The experimental $H_5O_2^+$·Ne spectrum shows two clearly distinguishable bands at similar positions to the 1741 and 1898 cm^{-1} absorptions in the MCTDH spectrum, as depicted in Fig. 2. The spectrum of $H_5O_2^+$·Ne also shows weak but non-negligible absorption in the region immediately above 1400 cm^{-1} (see Fig. 5 in Ref. 5).

Propagation of test states followed by Fourier analysis of their autocorrelation functions as described in Sec. II B were used to assign these peaks. The following test states were generated using eigenfunctions of low dimensional Hamiltonians: $|\Phi_{1z,1R}\rangle$, $|\Phi_{1z,2R}\rangle$, $|\Phi_{bu}\rangle$. The test state $|\Phi_{bu}\rangle$ consists on the water-bending with *ungerade* symmetry, i.e. it is characterized by $(|01\rangle - |10\rangle)/\sqrt{2}$ where the two entries indicate the quanta of bending motion of monomer A and B, respectively.

TABLE II AROUND HERE

The overlaps $|\langle\Phi|\Psi\rangle|^2$, where $|\Phi\rangle$ is a test state and $|\Psi\rangle$ is an eigenstate, are given in Tab. II. The analysis contemplates also the states of the doublet at 1000 cm^{-1}, since these states are coupled to some extent to the ones in the middle spectral-region, e.g., the eigenstate $|\Psi_d^h\rangle$ has a squared overlap of 0.10 with the test state $|\Phi_{bu}\rangle$. All states in Tab. II are of B_2^+ symmetry.

State $|\Psi_{m1}\rangle$, absorbing at 1411 cm^{-1} in the MCTDH spectrum, has a largest contribution from the $|\Phi_{1z,1R}\rangle$ test state. The experimental $H_5O_2^+$·Ne spectrum shows a weak absorption in this region with a lower intensity than the peaks at 1763 and 1878 cm^{-1}, the same trend as in the MCTDH spectrum. Based on the general good agreement between the experimental and MCTDH spectra we propose that this weak absorption is mainly a combined excitation $(1z, 1R)$. A band appearing at 1600 cm^{-1} in the MM/VCI spectrum [5] was assigned to the $(1z, 1R)$ transition. However, the experimental spectrum of $H_5O_2^+$·Ne shows no absorption at 1600 cm^{-1} [5].

State $|\Psi_{m2}\rangle$, which is responsible for the absorption at 1741 cm^{-1} in the MCTDH spectrum, has the largest contribution from the $|\Phi_{bu}\rangle$ test state. This peak is then mainly related to the *ungerade* water-bending, and has been already assigned in Ref. 5 and a number of works. This peak can be assigned already from a standard normal-modes analysis, since its main contribution is from an internal motion of the water monomers, and less from the relative motions between them. However, it must not come as a surprise that the eigenstate $|\Psi_{m2}\rangle$ has a total squared overlap of 0.26 with the test states containing one quanta of excitation in the proton transfer coordinate, namely $|\Phi_{1z}\rangle$, $|\Phi_{1z,1R}\rangle$ and $|\Phi_{1z,2R}\rangle$. In a fashion similar to the coupling to the w_3 wagging motion, as the proton approaches one water molecule the equilibrium value of the H-O-H angle shifts to a larger value because this water molecule acquires more H_3O^+ character. Conversely, the water molecule at a larger distance of the central proton acquires H_2O character and the angle H-O-H shifts to lower values.

State $|\Psi_{m3}\rangle$ is responsible for the absorption at 1898 cm^{-1} in the MCTDH spectrum, the lowest intensity feature of the doublet centered at about 1800 cm^{-1}. This state has the largest overlap with the $|\Phi_{1z,2R}\rangle$ test-state. Comparison in position and intensity of this peak to the corresponding one in the experimental $H_5O_2^+$·Ne spectrum suggests that the latest is mainly related to the $(1z, 2R)$ excitation.

Analysis of the values in Tab. II shows that the eigenstates in the region 1400-1900 cm^{-1} are characterized by the asymmetric bending and combinations of the proton-transfer fundamental and water-water-stretch fundamental and first overtone, with important couplings between them. Such a coupling was already noted by Bowman and collaborators by analyzing the CI coefficients of their MM/VCI expansion [5]. However, the exact nature of each band could not be disentangled, and it was concluded that this "is indicative of large cou-

plings among various zero-order states in this region". We show that, despite such couplings exist and play an important role in shaping the spectrum, the different eigenstates involved retain each its particular character (note that the largest numbers in Tab. II appear at the diagonal) and can be assigned to well defined transitions.

D. 2000-4000 cm^{-1} region

Symmetry analysis of the OH stretchings of the water molecules within the $\mathcal{G}_{16}$ group predicts four vibrational states with labels A_1^+, B_2^+ and E^+, and the corresponding torsional splitting A_1^-, B_2^- and E^- states. The states-labeling simplifies to A_1, B_2 and E, respectively, when adopting the $\mathcal{D}_{2d}$ point group, in which the internal rotation around α is treated as unfeasible. The use of the smaller group $\mathcal{D}_{2d}$ is reasonable here because all the minus-states are dark in the linear IR-spectrum. The A_1 state corresponds to the symmetrical, *gerade* stretch, the B_2 state is the symmetrical, *ungerade* stretch and the E states are the two asymmetrical stretches of *gerade* and *ungerade* type. We recall that the notation *gerade/ungerade* is used to indicate $+/-$ linear combinations of the motions of the two monomers, while symmetric/antisymmetric refers to the OH motions *within* each monomer. A symmetry analysis based on the $\mathcal{C}_2$ point group, the symmetry group of the absolute minimum, labels the symmetric stretches as A and B states and the asymmetric stretches again as A and B states. The harmonic analysis results (see Tab I) yield the symmetric stretches separated by less than 10 cm^{-1} and appear at a lower energy than the asymmetric stretches. The asymmetric stretches, despite not being degenerate, are very close in energy, separated by less than 1 cm^{-1}. Exact degeneracy of the asymmetric stretches is regained as a consequence of the feasibility of the wagging-motions, leading to $\mathcal{D}_{2d}$ symmetry.

The MCTDH spectrum in the water-stretching region reveals two absorptions. The lowest energy one is related exclusively to the z component of the dipole, while the largest energy, most intense band arises exclusively from the perpendicular component (seen Fig. 1). The lowest energy absorption is related to the symmetric, *ungerade* stretching, while the highest energy absorption is related to the degenerate asymmetric stretchings. The energy separation between symmetric and asymmetric stretchings is known to be of about 80 cm^{-1} as seen from different experiments and computations [5, 31], so these peaks can be resolved by a propagation of about 260 fs. The splitting between symmetric *gerade* and *ungerade* stretch-

ings is expected to be less than 10 cm^{-1} according to harmonic results. Thus, a propagation of about 2100 fs would be needed to resolve these peaks, which is unfeasible in a reasonable amount of computer time for this system. In order to resolve the symmetric stretchings two initial test-states were prepared by diagonalization of mode-operators, the symmetric *gerade* ($|\Phi_{sg}\rangle$) and symmetric *ungerade* ($|\Phi_{su}\rangle$) stretchings. Both test states were propagated and their auto- and crosscorrelation functions analyzed by means of the FD method. FD analysis yields the symmetric, in-phase stretching at 3607 cm^{-1}, and the symmetric, out-of-phase counterpart at 3614 cm^{-1}. Propagation of a test state $|\Phi_{sa}\rangle$ of the asymmetric, doubly degenerate stretchings yields the peak centered at 3689 cm^{-1}. These results are in excellent agreement to the bands observed in the experimental $H_5O_2^+$·Ne spectrum [5]. Note that the propagation of $|\Phi_{sa}\rangle$ yields a result in better agreement to experiment than the peak in Fig. 2 obtained by propagation of the perpendicular component of the dipole. This is due to the fact that the wavefunction obtained from application of the dipole operator to the ground state is a coherent superposition of several eigenstates that are propagated together. The more eigenstates are to be coherently propagated, the more complex is the dynamics of the wavepacket and the less accurate becomes the propagation for each individual state. For this reason, the most accurate energies (e.g. values in Table I) are obtained from either *improved relaxation* to the desired eigenstate, if possible, or propagation of carefully prepared wavepackets (referred to as test states in this work) which have as much overlap as possible with the eigenstate of interest or a group of them. As a final remark, the spectrum arising from direct excitation of the z coordinate (propagation of the $|\Phi_{1z}\rangle$ test state) yields all the peaks in the range 800-2000 cm^{-1} with almost the same relative intensities than compared to the propagation of $\mu_z|\Psi_0\rangle$. However, the propagation of $|\Phi_{1z}\rangle$ gives a completely flat spectrum in the region above 3000 cm^{-1}. This indicates that the excitation of the stretching motions must occur locally on each water molecule and does not depend on the excitation of the central proton. Moreover, the coupling of the stretching motions to the central proton is very weak, as indicated by the splitting of only 7 cm^{-1} between *gerade* and *ungerade* symmetric stretchings and indicates that the OH stretchings of $H_5O_2^+$ are robust to the displacement of the central proton, contrary to the situation seen for wagging and bending modes. Despite the excitation of the stretchings is local in each water monomer, the calculated band at 3614 cm^{-1} corresponds to the symmetric, *ungerade* mode of B_2 symmetry, since both water molecules are oriented in opposite directions with

respect to the z-direction incident field. The symmetric, *gerade* mode is a dark state of A_1 symmetry.

IV. SUMMARY AND CONCLUSION

The infrared absorption spectrum of the Zundel cation ($H_5O_2^+$) is calculated by the quantum-dynamical multiconfiguration time-dependent Hartree (MCTDH) method in the linear-absorption spectral-range $0 - 4000$ cm^{-1}. The energies of all fundamentals and several overtones related to different motions of the system are reported. The cation is considered in its full dimensionality (15D). A curvilinear set of coordinates is used to describe the configuration of the system. Details on the derivation of the kinetic energy operator used, which is exact for total angular momentum $J = 0$, and on the representation of the potential energy surface are given in the companion paper [15].

The lowest frequency part of the spectrum, shows a strong absorption at about 100 cm^{-1} due to the combination of the fundamental wagging-modes w_1, which are E^- degenerate states, and the internal-rotation state (1α) of A_1^- symmetry. The resulting pair of degenerate states is of E^+ symmetry and therefore bright. The two absorptions at 250 and 500 cm^{-1} are related to the combination state of the fundamental waggings and the (3α) state, which results in a pair of E^+ degenerate states and to the rocking fundamentals, also of E^+ symmetry, respectively. These absorptions are related to the component of the field perpendicular to the water-water axis. The spectral region at about 1000 cm^{-1} presents a double-peak absorption which is the most characteristic feature of the spectrum. This double peak is seen to arise from the coupling of the proton-transfer motion with a combination state involving the w_3 wagging mode. The reduced probability density of the w_3 wagging mode projected onto the wagging coordinates is shown in Fig. 5b. This state presents four probability maxima, each of which corresponds to a water in pyramidal conformation (H_2O character) while the other is in planar conformation (H_3^+O character), and has an energy of 374 cm^{-1}. This state alone absorbs light only very weakly (see Fig. 1), but the state arising from the combination of w_3 and the water-water stretching (550 cm^{-1}) reaches an energy close to the natural absorption of the proton-transfer at about 1000 cm^{-1}. The coupling between these both states explains the doublet absorption at about 1000 cm^{-1}, which is interpreted as a Fermi resonance between the combination state ($1R$,w_3) and the

proton-transfer fundamental ($1z$).

The region between 1000 and 2000 cm^{-1} presents three main absorptions at 1411, 1741 and 1898 cm^{-1}. The peak with the highest intensity in this region is the peak at 1741 cm^{-1} which corresponds to the *ungerade* bending motion of the water moieties. The eigenstate at 1741 cm^{-1} has in addition important contributions from the proton-transfer mode and proton transfer combined with the water-water stretching mode (see Tab. II). The eigenstates absorbing at 1411 and 1898 cm^{-1} are both described by one quantum on the proton-transfer mode plus one and two quanta excitations, respectively, on the water-water stretching mode. The nature of the two eigenstates of the doublet at 1000 cm^{-1} and the three eigenstates between 1000 and 2000 cm^{-1} is described by clearly defined motions (diagonal elements in Tab. II), e.g. the asymmetric bending. However, they constitute a set of coupled states (non-diagonal elements in Tab. II) featuring the wagging, bending, water-water stretch and proton-transfer motions.

The region above 3000 cm^{-1} presents the direct absorptions of the OH-stretching motions starting at about 3600 cm^{-1}. Symmetry analysis of the OH-stretching motions in the $\mathcal{D}_{2d}$ or $\mathcal{G}_{16}$ groups reveals that the symmetric *gerade* and *ungerade* stretching transform according to the A_1 and B_2 representations, respectively. The *ungerade*, B_2 state absorbs at 3614 cm^{-1} due to the z-component of the field. The *gerade*, A_1 state, which is dark, has an energy of 3607 cm^{-1}. The small energy splitting between *gerade* and *ungerade* states shows that the coupling of these motions to the central proton motion must be very weak. Furthermore, our analysis also points out that the excitation of the *ungerade*, B_2 state is completely independent of the central proton excitation, and is caused by interaction of the field with the local dipole of each monomer. Symmetry analysis reveals also that the asymmetric *gerade* and *ungerade* states are E degenerate. They absorb at 3689 cm^{-1} due to the component of the field perpendicular to the water-water axis.

The fact that the $H_5O_2^+$ cation may interconvert between several low energy barriers connecting equivalent minima had already been pointed out by Wales [29], who showed that the correct symmetry group, because wagging and internal rotation motions are allowed, is the permutation-inversion group $\mathcal{G}_{16}$ [33]. Our study shows that the symmetry analysis in $\mathcal{G}_{16}$ is necessary to understand some important features of the IR linear absorption spectrum. In addition, it has been shown in Paper I that already in the ground vibrational state there is non-neglible probability of crossing the internal-rotation barrier. However, the consideration

of the cation in the more familiar $\mathcal{D}_{2d}$ point group may provide an adequate labelling of the vibrational motions of the system as long as the internal-rotation mode is not involved in the considered states.

The reported calculations are in excellent agreement to the experimental measurements of Ref. [5] on the predissociation spectrum of $H_5O_2^+ \cdot Ne$. The discrepancy of the MCTDH energies reported in Tab. I with respect to the position of the measured bright bands lies always below 22 cm^{-1}, the average discrepance is 14 cm^{-1} (see Tab. I). Such a remarkable consistency between experiment and theory along the whole spectral range represents, on the one hand, a validation of the underlying potential energy surface of Huang *et al.* [11] and of the mode-based cluster expansion of the potential [15] used in the quantum-dynamical simulations, but is also a clear indication that a suitable set of coordinates was selected to tackle the problem [15]. On the other hand, it provides a validation of the measurements on the $H_5O_2^+ \cdot Ne$ cation by the predissociation technique, since this method gives access to the infrared linear-absorption regime without noticeable disturbances caused by the messenger atom. The only essential disagreement between experiment and theory is in the intensities. The intensities are not measured absolutely but, in comparison to the bright double-peak at 1000 cm^{-1}, the structures which appear between 1400 and 2000 cm^{-1} are too low by a factor of 3 when compared to the MCTDH simulation. Such a discrepancy does not occur in the spectrum of $H_5O_2^+ \cdot Ar$ [5], which displays a relative intensity in that region similar to the MCTDH one despite an incorrect shape. Therefore we conclude that more investigations are necessary to determine the origin of the discrepancy in relative intensities between experiment and theory in some regions of the spectrum.

The fact that the reported simulations are successful in obtaining accurate results for a system of the dimensionality of the protonated water-dimer is to be attributed in great part to the MCTDH algorithm, in which not only the expansion coefficients, but also the orbitals (here SPFs), are variationally optimal. For a 15-dimensional system the use of only 4 basis functions per degree of freedom represents of the order of 10^9 configurations. The largest calculations reported here consist of about 10^7 configurations, while already good results are obtained by using as few as 10^5 configurations (see Tab. 3 in Paper I). Such an *early* convergence of the MCTDH method becomes crucial as high-dimensional problems are attempted.

The reported simulations constitute a new example of the ability of the MCTDH method

to tackle high dimensional, complex molecular systems in a rigorous manner, and they open exciting perspectives for the simulation and understanding of even more complicated systems by means of accurate, non-trivial quantum-dynamical methods. Last but not least, they provide important information on the spectroscopy and dynamics of the hydrated proton.

V. ACKNOWLEDGMENTS

The authors thank Prof. J. Bowman for providing the potential-energy routine, M. Brill for the help with the parallelized code, and the Scientific Supercomputing Center Karlsruhe for generously providing computer time. O. V. is grateful to the Alexander von Humboldt Foundation for financial support. Travel support by the Deutsche Forschungsgemeinschaft (DFG) is also gratefully acknowledged.

---

[1] D. Marx, M. Tuckerman, J. Hutter, and M. Parrinello, Nature **397**, 601 (1999).

[2] N. Agmon, Isr. J. Chem. **39**, 493 (1999).

[3] J.-C. Jiang, Y.-S. Wang, H.-C. Chang, S. H. Lin, Y. T. Lee, G. Niedner-Schatteburg, and H.-C. Chang, J. Am. Chem. Soc. **122**, 1398 (2000).

[4] J. M. Headrick, E. G. Diken, R. S. Walters, N. I. Hammer, R. A. Christie, J. Cui, E. M. Myshakin, M. A. Duncan, M. A. Johnson, and K. D. Jordan, Science **308**, 1765 (2005).

[5] N. I. Hammer, E. G. Diken, J. R. Roscioli, M. A. Johnson, E. M. Myshakin, K. D. Jordan, A. B. McCoy, X. Huang, J. M. Bowman, and S. Carter, J. Chem. Phys. **122**, 244301 (2005).

[6] K. R. Asmis, N. L. Pivonka, G. Santambrogio, M. Brummer, C. Kaposta, D. M. Neumark, and L. Woste, Science **299**, 1375 (2003).

[7] T. D. Fridgen, T. B. McMahon, L. MacAleese, J. Lemaire, and P. Maitre, J. Phys. Chem. A **108**, 9008 (2004).

[8] J. M. Headrick, J. C. Bopp, and M. A. Johnson, J. Chem. Phys **121**, 11523 (2004).

[9] M. V. Vener, O. Kühn, and J. Sauer, J. Chem. Phys. **114**, 240 (2001).

[10] J. Dai, Z. Bacic, X. C. Huang, S. Carter, and J. M. Bowman, J. Chem. Phys. **119**, 6571 (2003).

[11] X. Huang, B. J. Braams, and J. M. Bowman, J. Chem. Phys. **122**, 044308 (2005).

[12] J. Sauer and J. Dobler, Chem. Phys. Chem. **6**, 1706 (2005).

[13] M. Kaledin, A. L. Kaledin, and J. M. Bowman, J. Phys. Chem. A **110**, 2933 (2006).

[14] O. Vendrell, F. Gatti, and H.-D. Meyer, Angewandte Chemie **in press** (2007).

[15] O. Vendrell, F. Gatti, D. Lauvergnat, and H.-D. Meyer, J. Chem. Phys. (2007).

[16] U. Manthe, H.-D. Meyer, and L. S. Cederbaum, J. Chem. Phys. **97**, 3199 (1992).

[17] M. H. Beck, A. Jäckle, G. A. Worth, and H.-D. Meyer, Phys. Rep. **324**, 1 (2000).

[18] H.-D. Meyer and G. A. Worth, Theor. Chem. Acc. **109**, 251 (2003).

[19] G. A. Worth, M. H. Beck, A. Jäckle, and H.-D. Meyer, The MCTDH Package, Version 8.2, (2000). H.-D. Meyer, Version 8.3 (2002), Version 8.4 (2007). See http://www.pci.uni-heidelberg.de/tc/usr/mctdh/.

[20] G. G. Balint-Kurti, R. N. Dixon, and C. C. Marston, J. Chem. Soc., Faraday Trans. **86**, 1741 (1990).

[21] H.-D. Meyer, F. Le Quéré, C. Léonard, and F. Gatti, Chem. Phys. **329**, 179 (2006).

[22] F. Richter, F. Gatti, C. Léonard, F. Le Quéré, and H.-D. Meyer, J. Chem. Phys. **in press** (2007).

[23] M. R. Wall and D. Neuhauser, J. Chem. Phys. **102**, 8011 (1995).

[24] M. H. Beck and H.-D. Meyer, J. Chem. Phys. **109**, 3730 (1998).

[25] M. H. Beck and H.-D. Meyer, J. Chem. Phys. **114**, 2036 (2001).

[26] F. Gatti, M. H. Beck, G. A. Worth, and H.-D. Meyer, PCCP **3**, 1576 (2001).

[27] H. C. Longuet-Higgins, Mol. Phys. **6**, 445 (1963).

[28] P. R. Bunker and P. Jensen, *Molecular Symmetry and Spectroscopy* (NRC Research Press, 1998), 2nd ed.

[29] D. J. Wales, J. Chem. Phys. **110**, 10403 (1999).

[30] J. M. Bowman, S. Carter, and X. Huang, Int. Rev. Phys. Chem. **22**, 533 (2003).

[31] L. I. Yeh, M. Okumura, J. D. Myers, J. M. Price, and Y. T. Lee, The Journal of Chemical Physics **91**, 7319 (1989),

[32] A. B. McCoy, X. Huang, S. Carter, M. Y. Landeweer, and J. M. Bowman, J. Chem. Phys. **122**, 061101 (2005).

[33] Note that Wales [29] uses a convention to assign irreducible representations which differs from the one we use [28]. The latter convention has the advantage to be consistent with the convention of the $\mathcal{D}_{2d}$ point group.

TABLE I: Vibrational-excited states as identified in the MCTDH calculations. Comparison is given to harmonic-analysis (HO) results in the same surface, the MM/VCI results and the experimental results on the $H_5O_2^+$·Ne cation. In the MCTDH column the subscript D indicates that the state was obtained by *improved relaxation* and the subscript F indicates that the state was identified by Fourier analysis. In the $|\langle\Psi_n|\hat{\mu}|\Psi_0\rangle|^2$ column, $\hat{\mu}$ refers to $\hat{\mu}_z$ for B_2^+ states and to $\hat{\mu}_x$ (or $\hat{\mu}_y$) for E^+ states. In the assignments column, in parenthesis, a number followed by a letter indicates the quanta of excitation in that coordinate. Other states are named after their definition in the text. As a remainder we note that w, r, b and s refer to wagging, rocking, bending and stretching. When meaningful a *ket* description of the state is given. In the *ket* description of the OH stretchings, S/A indicate symmetric/asymmetric stretching-motion within each monomer, respectively. The last column shows the irreducible representation of the $\mathcal{G}_{16}$ permutation-inversion group to which the vibrational state belongs. The irreducible representations of the more familiar point-group $\mathcal{D}_{2d}$, which is a subgroup of $\mathcal{G}_{16}$, are obtained by simply dropping the upper $(+/-)$ index.

Description	HO [a]	VCI(DMC) [b]	Exp. [c]	MCTDH [d]	assignment		$\lvert\langle\Psi_n\lvert\hat{\mu}\rvert\Psi_0\rangle\rvert^2$	$\mathcal{G}_{16}$
				$1_{(D)}$	(1α)		dark	A_1^-
Torsion	170			$103_{(D)}$	(2α)		dark	B_1^+
				$126_{(D)}$	(3α)		dark	B_1^-
				$210_{(F)}$	(4α)		dark	A_1^+
	339, 471			$106_{(D)}$	$w_{1a,b}$	$\lvert10\rangle \pm \lvert01\rangle$	dark	E^-
				$108_{(D)}$	$(1\alpha, w_{1a,b})$		0.126	E^+
Wagging				$232_{(D)}$	w_2	$\lvert11\rangle$	dark	B_1^+
				$254_{(F)}$	$(3\alpha, w_{1a,b})$		0.010	E^+
				$374_{(D)}$	w_3	$\lvert20\rangle - \lvert02\rangle$	0.0017	B_2^+
				$422_{(D)}$	w_4	$\lvert20\rangle + \lvert02\rangle$	dark	A_1^+
	532, 554			$481_{(F)}$	$r_{1a,b}$	$\lvert10\rangle \pm \lvert01\rangle$	0.0021	E^+
Rocking				$915_{(F)}$	r_2	$\lvert20\rangle + \lvert02\rangle$	dark	A_1^+
				$930_{(F)}$	r_3	$\lvert20\rangle - \lvert02\rangle$	0.0071	B_2^+
				$943_{(F)}$	r_4	$\lvert11\rangle$	dark	B_1^+
Wat-Wat str.	630			$550_{(D)}$	$(1R)$		dark	A_1^+
				$1069_{(D)}$	$(2R)$		dark	A_1^+
Proton-transfer			928	$918_{(F)}$	$(1R, w_3)$		0.042	B_2^+
doublet	861	1070(995)	1047	$1033_{(F)}$	$(1z)$		0.079	B_2^+
and overtone				$2338_{(F)}$	$(2z)$		dark	A_1^+
Proton perp.	1494, 1574			$1391_{(F)}$	$(1x)$,$(1y)$		0.00076	E^+
Proton-transfer +		1600	$\approx$ 1425	$1411_{(F)}$	$(1z, 1R)$		0.0064	B_2^+
Wat-Wat str.		1832/1910	1878	$1898_{(F)}$	$(1z, 2R)$		0.0063	B_2^+
Wat. bend (*gerade*)	1720	1604		$1606_{(F)}$	bg	$\lvert10\rangle + \lvert01\rangle$	dark	A_1^+
(*ungerade*)	1770	1781	1763	$1741_{(F)}$	bu	$\lvert10\rangle - \lvert01\rangle$	0.019	B_2^+
O-H (sym,*gerade*)	3744	3610(3511)		$3607_{(F)}$	sg	$\lvert S0\rangle + \lvert 0S\rangle$	dark	A_1^+
(sym,*ungerade*)	3750	3625(3553)	3603	$3614_{(F)}$	su	$\lvert S0\rangle - \lvert 0S\rangle$	0.0028	B_2^+
(asym)	3832	3698(3652)	3683	$3689_{(F)}$	sa	$\lvert A0\rangle \pm \lvert 0A\rangle$	0.0028	E^+

[a]Normal mode harmonic analysis. Results are taken from Ref. [11].

[b]Energies computed by the MULTIMODE program and (in parenthesis) by diffusion Monte-Carlo. Results taken grom Ref. [32].

[c]Experimental results taken from Ref. [32].

[d]This work.

TABLE II: Overlaps $|\langle\Phi|\Psi\rangle|^2$, where $|\Phi\rangle$ are test states and $|\Psi\rangle$ are eigenstates.

	$\|\Psi_d^l\rangle$	$\|\Psi_d^h\rangle$	$\|\Psi_{m1}\rangle$	$\|\Psi_{m2}\rangle$	$\|\Psi_{m3}\rangle$
Energy [cm^{-1}]	918	1033	1411	1741	1898
$\langle\Phi_{1R,w_3}\|$	0.83	0.09	0.00	0.00	0.00
$\langle\Phi_{1z}\|$	0.10	0.46	0.04	0.10	0.04
$\langle\Phi_{1z,1R}\|$	0.00	0.00	0.44	0.06	0.01
$\langle\Phi_{bu}\|$	0.07	0.12	0.10	0.38	0.02
$\langle\Phi_{1z,2R}\|$	0.00	0.00	0.00	0.10	0.38

Figure Captions

Figure 1: Simulated MCTDH spectrum in the range 0–4000 cm^{-1}. Excitation in the z direction (top), perpendicular to the O-H-O axis (middle) and total spectrum, i.e. $(1/3)z + (2/3)*$perpendicular (bottom). Note the different scale of intensities in the perpendicular-component plot. Autocorrelation time $T = 1000$ fs. Absorption is given in absolute scale in mega-barns (Mb). (1 Mb = 10^{-18} cm^2).

Figure 2: Comparison between the MCTDH spectrum (top) and the $H_5O_2^+ \cdot Ne$ spectrum of Ref. [5] (bottom). The intensity of the experimental spectrum is adjusted in each spectral region (800-2000 and 3500-3800 cm^{-1}) using the most intense peak of the MCTDH spectrum as a reference. Absorption for the MCTDH spectrum is given in absolute scale in mega-barns (Mb). (1 Mb = 10^{-18} cm^2).

Figure 3: Reduced probability density on the internal rotation α for (a) the ground state and the first three excited states: (b) 1α, (c) 2α and (d) 3α. The dotted lines correspond to an enlarged scale ($\times 10$). The $+/-$ symbols are intended to clarify the symmetry properties of each state. They indicate the sign of the underlying wavefunction based on a 1D computation for coordinate α and do not refer directly to the multidimensional wavefunctions from which densities are given.

Figure 4: Reduced probability density on the wagging coordinates γ_A and γ_B of (a) the ground vibrational state and (b) the first-excited (w_{1a}) wagging-mode states.

Figure 5: Reduced probability density on the wagging coordinates γ_A and γ_B of the excited states w_2, w_3 and w_4, characterized by two quanta of excitation. Compare with Table I.

Figure 6: Schematic representation of the two most important coupled motions responsible for the doublet peak at 1000 cm^{-1}

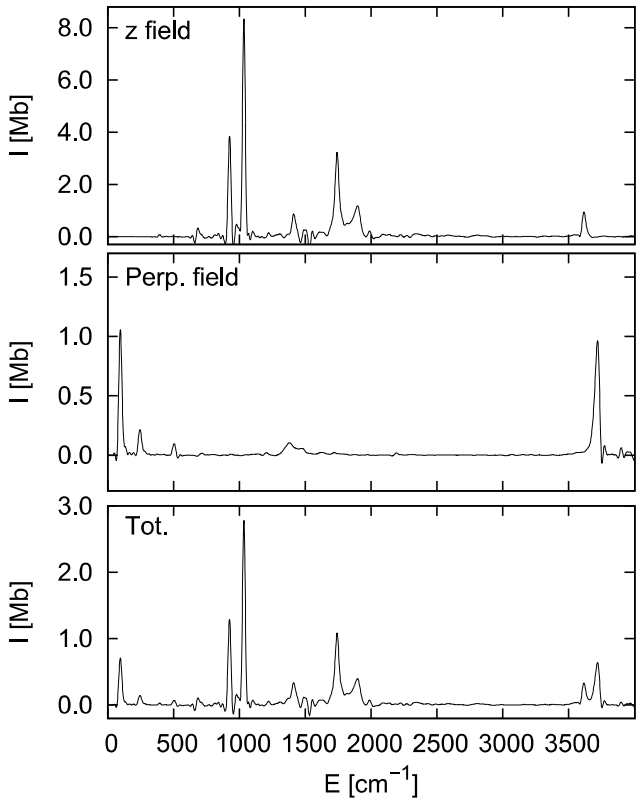

FIG. 1: Vendrell et. al., Journal of Chemical Physics

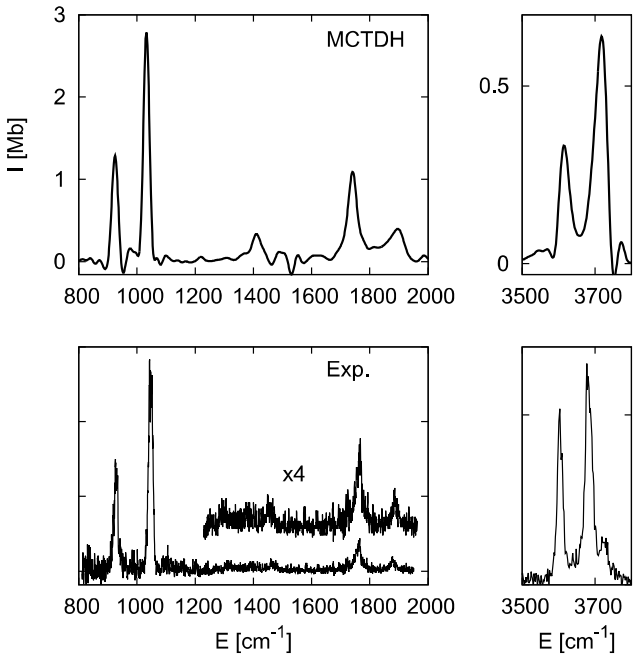

FIG. 2: Vendrell et. al., Journal of Chemical Physics

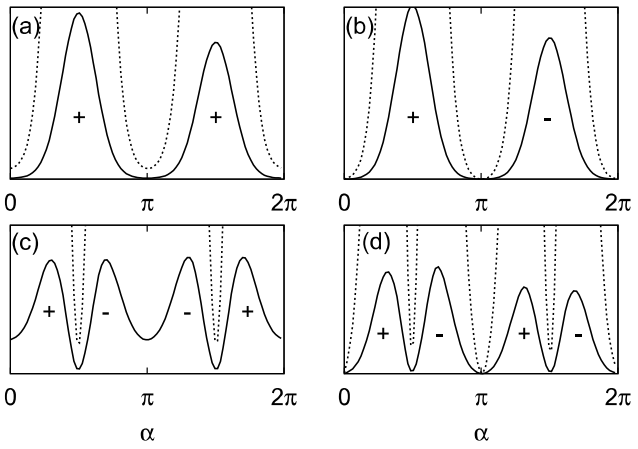

FIG. 3: Vendrell et. al., Journal of Chemical Physics

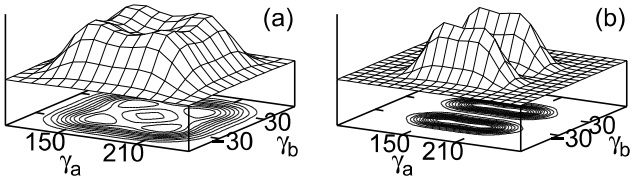

FIG. 4: Vendrell et. al., Journal of Chemical Physics

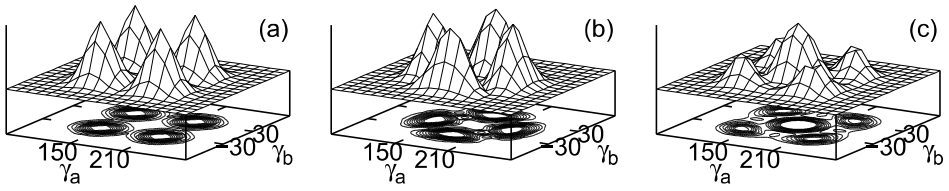

FIG. 5: Vendrell et. al., Journal of Chemical Physics

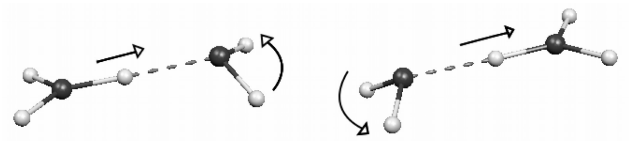

FIG. 6: Vendrell et. al., Journal of Chemical Physics